Chemical Engineering Science 269 (2023) 117541

Contents lists available at ScienceDirect

Chemical Engineering Science

journal homepage: www.elsevier.com/locate/ces

Physico-mathematical model for multiple ultrasound-contrast-agent microbubbles encapsulated by a visco-elastic shell: Effect of shell compressibility on ultrasound attenuation

Yusei Kikuchi [a], Tetsuya Kanagawa [b], Takahiro Ayukai [a]

[a] Department of Engineering Mechanics and Energy, Graduate School of Science and Technology, University of Tsukuba, Tsukuba 305-8573, Japan
[b] Department of Engineering Mechanics and Energy, Institute of Systems and Information Engineering, University of Tsukuba, Tsukuba 305-8573, Japan

HIGHLIGHTS

- Extension of acoustic theory for single encapsulated bubble to multiple bubbles.
- Bubble encapsulated by a visco-elastic shell with compressibility.
- Presence of shell affected advection, nonlinearity, and dissipation of ultrasound.
- Ultrasound dissipation by compressibility and viscosities of shell and liquid.
- Dissipation due to shell compressibility was the highest.

ARTICLE INFO

Article history:
Received 9 November 2021
Received in revised form 9 February 2022
Accepted 19 February 2022
Available online 24 February 2022

Keywords:
Encapsulated bubble
Ultrasound contrast agent
Bubble dynamics
Bubbly liquid
Weakly nonlinear theory
Visco-elastic shell

ABSTRACT

Owing to its potential for application in ultrasound-based diagnosis and therapy, the dynamics of a microbubble encapsulated by shells has long been theoretically investigated. However, outside of our research group, previous theories have been restricted to the case of single encapsulated bubble, whereas in practical diagnostic scenarios, multiple encapsulated bubbles are used as ultrasound contrast agents. In this study, the most recent theory for a single encapsulated bubble incorporating shell compressibility was extended for multiple encapsulated bubbles. Using the method of multiple scales, weakly nonlinear wave equation for one-dimensional ultrasound in liquids containing multiple encapsulated microbubbles was derived from the set of volumetric averaged equations for bubbly flow. It was found that the shell compressibility significantly increased the advection and dissipation effects of ultrasound. Further, five types of dissipation effects were compared with each other, and showed that the dissipation effects corresponding to shell compressibility were the highest.

1. Introduction

In recent decades, medical applications of ultrasound have received significant attention, leading to several developments in this area (e.g., ter Haar, 1999; Yoshizawa et al., 2009; Bader et al., 2016; Park et al., 2017; Kok et al., 2020; Uddin et al., 2021; Fateh et al., 2021). The use of microbubbles as the ultrasound contrast agent (UCA) drastically improves image resolution (e.g., Qin et al., 2009; Ignee et al., 2016; Chong et al., 2018; Zhu and Tagawa, 2019; de Leon et al., 2019). UCAs are used not only for echocardiography (Christiansen et al., 1994; Cohen et al., 1998) but also for the detection of liver cancer (Postema and Gilja, 2011). Recently, in addition to their intended use as contrast agents in medical imaging, the use of UCAs for therapeutic purposes has been explored [e.g., for transportation in drug delivery systems (DDS)] (Ferrara et al., 2007; Coussios and Roy, 2008; Lentacker et al., 2009; Choi et al., 2011; Kooiman et al., 2014; Roovers et al., 2019; Entzian and Aigner, 2021).

From a physical perspective, a precise understanding of the interaction between ultrasound propagation and the UCA (i.e., encapsulated microbubble) oscillations is desirable. Subharmonics and ultraharmonics as a nonlinear component of ultrasound, induced by nonlinear oscillations of UCA in an ultrasound field, are the basis of such medical technologies. In most UCAs, the gas

https://doi.org/10.1016/j.ces.2022.117541
0009-2509/

inside the bubble is stabilized against dissolution via encapsulation by a shell and membrane, among others (Sojahrood et al., 2021e). UCAs, such as Albunex and Sonazoid, have been utilized in clinical applications (Cosgrove and Harvey, 2009). The performance of the UCA depends on the properties of the shell and the incident acoustic pressure (Hoff et al., 2000; Sarkar et al., 2005). Attenuation and scattering experiments were performed using various types of UCAs to understand their properties (de Jong et al., 1992; Frinking and de Jong, 1998; Gorce et al., 2000; Morgan et al., 2000; Andersen and Jensen, 2009; Tu et al., 2009; Renaud et al., 2012; Tran et al., 2016; Yoshida et al., 2016). Molecular dynamics simulations have also been performed to determine the properties of the shell (Boek et al., 2005; van Opheusden and Molenaar, 2011). In addition, attempts have been made to model shell parameters based on molecular interactions (Stride, 2008; Borden, 2019). The group of Sojahrood extensively investigated the dynamics of encapsulated bubbles (including the free bubble case) through various aspects such as bifurcation structure (Sojahrood et al., 2015, 2021c, 2021f; Sojahrood and Kolios, 2012), sub- and superharmonic behaviors (Sojahrood et al., 2019, 2020a, 2021a, 2021d), and the mechanics of nonlinear power dissipation (Sojahrood et al., 2020b, 2020c, 2021b).

From the viewpoint of the equation of motion for UCA, many types of physico-mathematical models have been derived by modifying the equation of motion of a single free bubble (i.e., a single bubble without a shell) as follows (Chabouh et al., 2021; Chatterjee and Sarkar, 2003; Church, 1995; de Jong et al., 1992; Doinikov et al., 2009; Doinikov and Dayton, 2007; Gubaidullin et al., 2021a,b; Hoff et al., 2000; Lajoinie et al., 2017; Marmottant et al., 2005; Morgan et al., 2000; Paul et al., 2010; Raymond et al., 2014; Sarkar et al., 2005; Segers et al., 2016; Tsiglifis and Pelekasis, 2008; Sojahrood et al., 2018). The first attempt at modeling the encapsulation of the UCA was made by de Jong et al. (1992). Church (1995) provided a more rigorous theoretical model by treating the encapsulating shell as an incompressible Kelvin–Voigt model. Hoff et al. (2000) then reformulated on the assumption that the shell thickness is small enough compared to the bubble radius. Sarkar et al. (2005) developed a visco-elastic interface model for the encapsulation of a thin-shelled UCA. Marmottant et al. (2005) developed a model applicable to UCAs that considers the physical properties of a lipid monolayer coating on a gas microbubble. Following the latter study, other nonlinear models have been proposed with more complex rheological behaviors, such as strain softening and hardening (Tsiglifis and Pelekasis, 2008; Paul et al., 2010) or shear thinning (Doinikov et al., 2009). The most recent model, utilized in this paper, developed by Chabouh et al. (2021), considered shell compressibility, and showed that neglecting compressibility leads to underestimation of the shear modulus. Meanwhile, double encapsulated bubbles were treated by Liu et al. (2016) who formulated their interaction. However, these studies (Chabouh et al., 2021; Chatterjee and Sarkar, 2003; Church, 1995; de Jong et al., 1992; Doinikov et al., 2009; Doinikov and Dayton, 2007; Gubaidullin et al., 2021a,b; Hoff et al., 2000; Lajoinie et al., 2017; Liu et al., 2016; Marmottant et al., 2005; Morgan et al., 2000; Paul et al., 2010; Raymond et al., 2014; Sarkar et al., 2005; Segers et al., 2016; Tsiglifis and Pelekasis, 2008; Sojahrood et al., 2018) were restricted to single or low numbers of encapsulated bubbles. Thus, a basic theory for non-limited (i.e., high numbers of) encapsulated bubbles in relation to ultrasound propagation should be established in light of their general use in diagnostic applications of UCAs. Although Ma et al. (2004) reported one case of deriving a nonlinear evolution equation for ultrasound in liquids containing multiple encapsulated bubbles and estimated equivalent acoustic nonlinearity parameters from the perspective of nonlinear acoustics, several propagation properties of nonlinear ultrasound such as advection and dissipation effects have remained ambiguous in the field of fluid mechanics of two-phase mediums (i.e., bubbly liquid). Our previous work (Kikuchi and Kanagawa, 2021) was the first attempt to extend a previously established theory (Kanagawa et al., 2010; Yano et al., 2013), which studied ultrasound propagation in liquids containing multiple microbubbles without shells, to include shells.

The aim of the present study is to incorporate previously neglected a compressibility of the shell into our previous theory (Kikuchi and Kanagawa, 2021) for ultrasound propagation in liquids containing multiple encapsulated microbubbles. Instead of Hoff et al. (2000)'s model [or Church (1995)'s model], we used Chabouh et al. (2021)'s model that incorporated the shell compressibility for the first time, as an equation for the bubble oscillation of a single encapsulated bubble. Combining Chabouh et al. (2021)'s model and volumetric averaged equations for bubbly liquids, we have successfully derived the Korteweg–de Vries–Burgers (KdVB) equation as a physico-mathematical model for acoustic properties of multiple encapsulated bubbles. Based on the derived KdVB equation, the effect of certain properties of shell encapsulating bubble (e.g., compressiblity, shear modulus, viscosity) on the acoustic properties, such as advection, nonlinearity, and dissipation, were clarified. We then considered the significant influence of shell compressibility, which should not be neglected. Typical UCAs (Albunex, SonoVue, Levovist, and Optison) were evaluated by comparing the coefficients in the KdVB equation. This is the first study on the effects of both multiple encapsulated bubbles and shell compressibility on ultrasound propagation.

The remainder of this paper is organized as follows. Section 2 introduces the basic equations for bubbly flow based on volumetric averaged equations (Ishii, 1977; Kataoka, 1991), and encapsulated bubble dynamics, including shell compressibility (Chabouh et al., 2021). Section 3 presents the derivation of the KdVB equation and explores the effect of shell compressibility on dissipation. The significant influence of shell compressibility on The propagation properties of ultrasound is then discussed. Finally, Section 4 concludes the paper.

2. Formulation of the problem

2.1. Problem statement

Consider a weakly nonlinear [i.e., finite but small amplitude (e.g., Jeffrey and Kawahara, 1982)] propagation of plane (one-dimensional), progressive pressure (or ultrasonic) waves radiated from a sound source placed in flowing liquids containing a uniform quantity of multiple spherical encapsulated bubbles. The number of encapsulated bubbles is sufficiently high to use the continuum model shown in Eqs. (4) and (5) below. For simplicity, the following assumptions are made:

(i) The compressibility of shell is newly incorporated. Although the shell compressibility changes the thickness of shell, the shell thickness is assumed to be a constant d_0^*, for simplicity.
(ii) The shell of the bubble is assumed to be a visco-elastic body (Kelvin–Voigt model).
(iii) The liquid is compressible.
(iv) Initially, the gas and liquid phases flow with a constant uniform velocity, and nonuniform velocity distribution of each phase (Maeda and Kanagawa, 2020) is not considered.

(v) The bubbles do not coalesce, break up (Lau et al., 2014), appear, or disappear, and bubble–bubble interaction (Fuster et al., 2014; Guédra et al., 2017; Haghi et al., 2019; Ma et al., 2015; Sojahrood et al., 2021a) is neglected.
(vi) The bubble oscillations are spherically symmetric.
(vii) The thermal conductivity (e.g., Prosperetti, 1991; Kamei et al., 2021; Kanagawa and Kamei, 2021; Kagami and Kanagawa, 2022) and phase change (e.g., Zhang and Li, 2014; Tryggvason and Lu, 2015; Kerboua et al., 2021) are neglected because the role of the thermal effect may not be essential in diagnostic applications.
(viii) The mass transport across the bubble–liquid interface (Hissanaga et al., 2020) is neglected (see Figs. 1 and 2).
(ix) The dissipation due to lift (Sankaranarayanan and Sundaresan, 2002; Dijkhuizen et al., 2010) and drag force (Arai et al., 2022; Kanagawa et al., 2021a; Yatabe et al., 2021) acting bubble is neglected.
(x) Multi-dimensionality (e.g., Kanagawa, 2015; Kanagawa et al., 2011) is not considered.

With the exception of (i), (iil), and (iv), these assumptions are identical to those in our previous work (Kikuchi and Kanagawa, 2021).

The shell of each encapsulated bubble is assumed to be a visco-elastic (Kelvin–Voigt model) body. Chabouh et al. (2021)'s model for bubble oscillations for a single encapsulated bubble [Eq. (1) below] is then installed for the equation of motion instead of Hoff et al. (2000)'s model.

2.2. Basic equations

Rather than the Hoff et al. (2000) or Church (1995) model, Chabouh et al. (2021)'s model was utilized as the equation of motion for spherically symmetric oscillations of an encapsulated bubble. This model incorporates the effect of a visco-elastic shell as a Kelvin–Voigt model and considers shell compressibility:

$$\rho_{\mathrm{L}0}^{*}\left(1-\frac{1}{c_{\mathrm{L}0}^{*}}\frac{\mathrm{D}R^{*}}{\mathrm{D}t^{*}}\right)R^{*}\frac{\mathrm{D}^{2}R^{*}}{\mathrm{D}t^{*2}}+\frac{3}{2}\rho_{\mathrm{L}0}^{*}\left(1-\frac{1}{3c_{\mathrm{L}0}^{*}}\frac{\mathrm{D}R^{*}}{\mathrm{D}t^{*}}\right)\left(\frac{\mathrm{D}R^{*}}{\mathrm{D}t^{*}}\right)^{2} = \left(1+\frac{1}{c_{\mathrm{L}0}^{*}}\frac{\mathrm{D}R^{*}}{\mathrm{D}t^{*}}\right)P^{*}+\frac{R^{*}}{c_{\mathrm{L}0}^{*}}\frac{\mathrm{D}}{\mathrm{D}t^{*}}\left(p_{\mathrm{L}}^{*}+P^{*}\right), \tag{1}$$

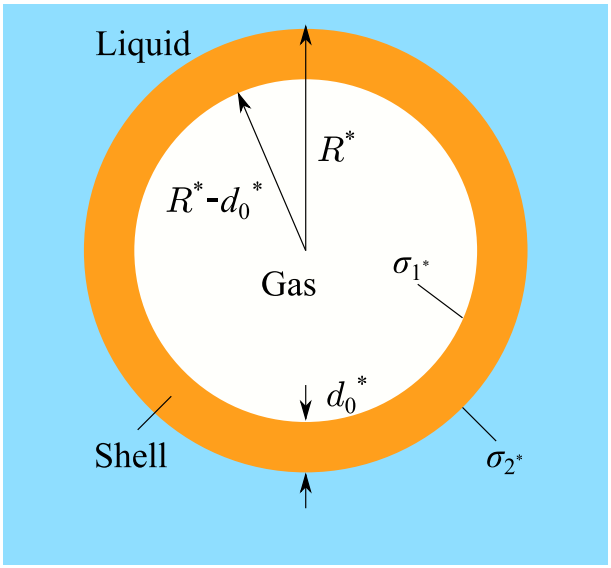

Fig. 2. Conceptual illustration of an encapsulated bubble; R^* is the bubble radius, d_0^* is the initial shell thickness, and σ_1^* and σ_2^* are the respective surface tensions at the internal and external boundaries of the shell.

with the balance relation of normal stresses,

$$\begin{aligned} P^{*} = {} & \left(p_{\mathrm{G}}^{*}-\frac{2\sigma_{1}^{*}}{R^{*}-d_{0}^{*}}\right)\left(1-\frac{4G^{*}}{3K^{*}+4G^{*}}\frac{3d_{0}^{*}}{R^{*}}\right)-p_{\mathrm{L}}^{*}-\frac{4\mu_{\mathrm{L}}^{*}}{R^{*}}\frac{\mathrm{D}R^{*}}{\mathrm{D}t^{*}} \\ & -12G^{*}\frac{3K^{*}}{3K^{*}+4G^{*}}\frac{d_{0}^{*}}{R^{*}}\left(1-\frac{R_{0}^{*}}{R^{*}}\right)-4\mu_{\mathrm{S}}^{*}\left(1-\frac{4G^{*}}{3K^{*}+4G^{*}}\right)\frac{d_{0}^{*}}{R^{*}\left(R^{*}-d_{0}^{*}\right)}\frac{\mathrm{D}R^{*}}{\mathrm{D}t^{*}} \\ & -8\mu_{\mathrm{K}}^{*}\frac{3G^{*}}{3K^{*}+4G^{*}}\frac{d_{0}^{*}}{R^{*}\left(R^{*}-d_{0}^{*}\right)}\frac{\mathrm{D}R^{*}}{\mathrm{D}t^{*}}-\frac{2\sigma_{2}^{*}}{R^{*}}. \end{aligned} \tag{2}$$

Here, the material derivative operator $\mathrm{D}/\mathrm{D}t^*$ is

$$\frac{\mathrm{D}}{\mathrm{D}t^{*}}=\frac{\partial}{\partial t^{*}}+u^{*}\frac{\partial}{\partial x^{*}}, \tag{3}$$

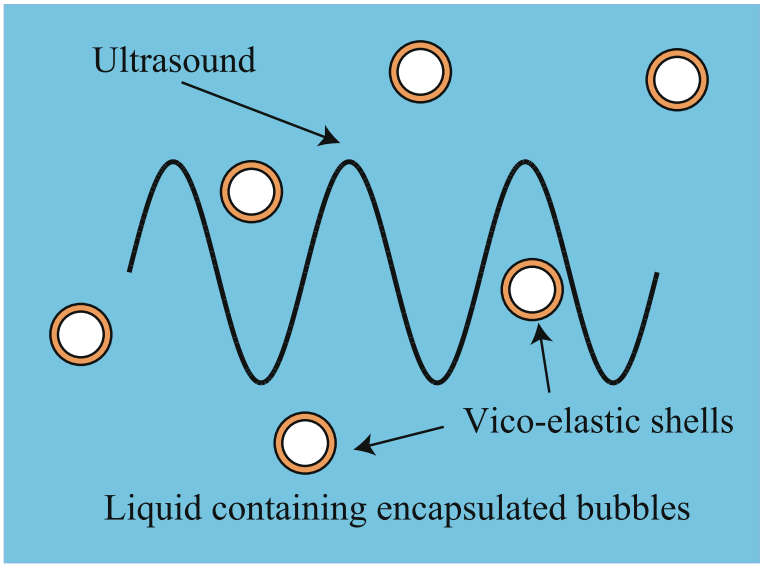

Fig. 1. Ultrasound propagation in liquid containing multiple spherical microbubbles encapsulated by a visco-elastic shell.

where t^* is the time and x^* is the space coordinate normal to the wave front; R^* is the bubble radius, p_G^* and p_L^* are the respective volumetric averaged pressures of gas and liquid phases, and P^* is a surface averaged liquid pressure; the superscript $*$ denotes dimensional quantity, the subscript 0 denotes the initial unperturbed state (e.g., R_0^* is the initial bubble radius), and G and L denote the respective gas and liquid phases; as constants, c_{L0}^* is sound speed in the unperturbed liquid, G^* is the shear modulus of shell, K^* is the bulk modulus of shell, μ_S^* is the shear viscosity of shell, μ_K^* is the viscosity describing the friction losses due to volume change of shell, ρ_{L0} is the initial liquid density, p_{G0}^* is the initial gas pressure, μ_L^* is the liquid viscosity, and d_0^* is the (initial) shell thickness. Here, σ_1^* and σ_2^* are the respective surface tensions at the internal and external boundaries of the shell. Eq. (1) was extended from a single bubble to the case of multiple bubbles; that is, $R^* = R^*(x^*, t^*)$ is treated as a field variable. In the case without a shell, Eq. (1) coincides with the Keller–Miksis equation for an uncoated bubble.

There are three unknown variables, i.e., R^*, p_L^*, and P^* in Eq. (1). The following equations for a flow field are then used to close the set of equations. The following conservation equations of mass and momentum for bubbly liquids based on the mixture model are used as volumetric averaged equations, which assumed the presence of multiple bubbles (Ishii, 1977; Kataoka, 1991):

$$\frac{\partial \rho^*}{\partial t^*} + \frac{\partial \rho^* u^*}{\partial x^*} = 0, \tag{4}$$

$$\frac{\partial \rho^* u^*}{\partial t^*} + \frac{\partial \rho^* u^{*2}}{\partial x^*} + \frac{\partial p_L^*}{\partial x^*} - \frac{4}{3}\mu^* \frac{\partial^2 u^*}{\partial x^{*2}} = 0, \tag{5}$$

where u^* is the fluid velocity. Here, it is assumed that the pressure of the bubbly liquid is equivalent to the average pressure of the liquid (Akhatov et al., 1994; Yano et al., 2013). The bubbly liquid is assumed to be a Newtonian fluid, and the viscosity of bulk liquid is ignored based on the Stokes assumption. As has been derived in several prior works (Schowalter et al., 1968; Choi and Schowalter, 1975), the viscosity of the bubbly liquid as a physical property, μ^*, is expressed as follows:

$$\mu^* = (1 + \alpha_0)\mu_L^*, \tag{6}$$

where α_0 is the initial void fraction. Here, μ^* is higher than μ_L^* because the mechanical work acting on the water and the velocity of the flow field are reduced owing to the containing bubbles (Einstein, 1906). Note that Eq. (6) is applicable if $\alpha_0 < 0.05$ (Murai et al., 2015). The volume-averaged density of the bubbly liquid ρ^* is defined as follows:

$$\rho^* = (1 - \alpha)\rho_L^*, \tag{7}$$

where α is the void fraction (i.e., volumetric fraction of gas phase; $0 < \alpha < 1$) and the density of the gas is neglected. The void fraction, α, is related to the number density of the bubbles, N^*, using the following equation:

$$\alpha = \frac{4}{3}\pi R^{*3} N^*, \tag{8}$$

$$\frac{\partial N^*}{\partial t^*} + \frac{\partial N^* u^*}{\partial x^*} = 0. \tag{9}$$

Eq. (8) defines α and Eq. (9) represents the conservation of N^*.

Substituting the following conservation equation of mass inside the bubble,

$$\frac{\rho_G^*}{\rho_{G0}^*} = \left(\frac{R_0^*}{R^*}\right)^3, \tag{10}$$

and Eq. (8) into Eq. (9), we obtain

$$\frac{\partial}{\partial t^*}(\alpha \rho_G^*) + \frac{\partial}{\partial x^*}(\alpha \rho_G^* u^*) = 0. \tag{11}$$

Furthermore, substituting Eqs. (6) and (7) into Eqs. (4) and (5), we obtain

$$\frac{\partial}{\partial t^*}[(1-\alpha)\rho_L^*] + \frac{\partial}{\partial x^*}[(1-\alpha)\rho_L^* u^*] = 0, \tag{12}$$

$$\frac{\partial}{\partial t^*}[(1-\alpha)\rho_L^* u^*] + \frac{\partial}{\partial x^*}[(1-\alpha)\rho_L^* u^{*2}] + \frac{\partial p_L^*}{\partial x^*} - \frac{4}{3}(1+\alpha_0)\mu_L^* \frac{\partial^2 u^*}{\partial x^{*2}} = 0. \tag{13}$$

The set of Eqs. (1) and (11)–(13) is closed by the Tait equation of state for the liquid phase and the polytropic equation of state for the gas phase, as follows:

$$p_L^* = p_{L0}^* + \frac{\rho_{L0}^* c_{L0}^{*2}}{n}\left[\left(\frac{\rho_L^*}{\rho_{L0}^*}\right)^n - 1\right], \tag{14}$$

$$\frac{p_G^*}{p_{G0}^*} = \left(\frac{\rho_G^*}{\rho_{G0}^*}\right)^\gamma, \tag{15}$$

where n is the material constant (e.g., $n = 7.15$ for water).

2.3. Multiple scale analysis

Independent variables are first nondimensionalized as

$$t = \frac{t^*}{T^*}, \quad x = \frac{x^*}{L^*}, \tag{16}$$

where T^* and L^* represent a typical period and wavelength of the concerned wave, respectively. Based on the method of multiple scales (e.g., Jeffrey and Kawahara, 1982), by the use of the nondimensionalized independent variables t and x, a near-field [i.e., the temporal and spatial scales of $O(1)$] is described by

$$t_0 = t, \quad x_0 = x, \tag{17}$$

and a far-field [i.e., the temporal and spatial scales of $O(1/\epsilon)$] is described by

$$t_1 = \epsilon t, \quad x_1 = \epsilon x, \tag{18}$$

where ϵ is a nondimensional wave amplitude that is sufficiently small compared to unity ($0 < \epsilon \ll 1$, i.e., a weakly nonlinear problem). Dependent variables are regarded as functions of the extended independent-variables in Eqs. (17) and (18). Thus, the differential operators are expanded as the manner of derivative expansion method (e.g., Jeffrey and Kawahara, 1982):

$$\frac{\partial}{\partial t} = \frac{\partial}{\partial t_0} + \epsilon \frac{\partial}{\partial t_1}, \quad \frac{\partial}{\partial x} = \frac{\partial}{\partial x_0} + \epsilon \frac{\partial}{\partial x_1}. \tag{19}$$

All the dependent variables are nondimensionalized and expanded in the power series of ϵ (Kanagawa et al., 2010):

$$\frac{\alpha}{\alpha_0} = 1 + \epsilon\alpha_1 + \epsilon^2\alpha_2 + \cdots, \tag{20}$$

$$\frac{u^*}{U^*} = u_0 + \epsilon u_1 + \epsilon^2 u_2 + \cdots, \tag{21}$$

$$\frac{R^*}{R_0^*} = 1 + \epsilon R_1 + \epsilon^2 R_2 + \cdots, \tag{22}$$

$$\frac{\rho_L^*}{\rho_{L0}^*} = 1 + \epsilon^2\rho_{L1} + \epsilon^3\rho_{L2} + \cdots, \tag{23}$$

$$\frac{p_L^*}{\rho_{L0}^* U^{*2}} = p_{L0} + \epsilon p_{L1} + \epsilon^2 p_{L2} + \cdots, \tag{24}$$

where $U^* (\equiv L^*/T^*)$ is the typical propagation speed of the concerned wave. It should be noted that the expansion of ρ_G^* and p_G^* were determined from Eqs. (23) and (24). The effect of initial polydispersity (e.g., Kanagawa et al., 2021b; Segers et al., 2018) is neglected in this paper, for simplicity.

The target considered herein is a low-frequency long wave. To focus this band, the set of three nondimensional ratios among the physical parameters was determined as in Kanagawa et al. (2010):

$$\frac{U^*}{c_{\mathrm{L0}}^*} \equiv O(\sqrt{\epsilon}) \equiv V\sqrt{\epsilon}, \tag{25}$$

$$\frac{R_0^*}{L^*} \equiv O(\sqrt{\epsilon}) \equiv \Delta\sqrt{\epsilon}, \tag{26}$$

$$\frac{\omega^*}{\omega_{\mathrm{B}}^*} \equiv \frac{1}{T^*\omega_{\mathrm{B}}^*} \equiv O(\sqrt{\epsilon}) \equiv \Omega\sqrt{\epsilon}, \tag{27}$$

where V, Δ, and Ω are constants of $O(1)$ and are calculated by the values of other symbols, ω^* is a typical angular frequency, and ω_{B}^* is a natural angular frequency of linear spherical symmetric oscillations of a single encapsulated bubble obtained from Eq. (1) (Chabouh et al., 2021):

$$\begin{aligned}\omega_{\mathrm{B}}^{*2} &= \frac{3K^*+4G^*}{\rho_{\mathrm{L0}}^* R_0^{*2}}\left\{4G^*\frac{3K^*}{3K^*+4G^*}\frac{R_0^{*3}-\left(R_0^*-d_0^*\right)^3}{R_0^{*3}}\right.\\ &\quad\left.+\left(3\gamma p_{\mathrm{G0}}^* - \frac{2\sigma_1^*}{R_0^*-d_0^*}\right)\left[1-\frac{4G^*}{3K^*+4G^*}\frac{R_0^{*3}-\left(R_0^*-d_0^*\right)^3}{R_0^{*3}}\right]\right\}\\ &\quad\times\left[\left(3\gamma p_{\mathrm{G0}}^* - \frac{2\sigma_1^*}{R_0^*-d_0^*}\right)\frac{R_0^{*3}-\left(R_0^*-d_0^*\right)^3}{R_0^{*3}} + 4G^* + 3K^*\frac{\left(R_0^*-d_0^*\right)^3}{R_0^{*3}}\right]^{-1}\\ &\quad-\frac{2\sigma_2^*}{\rho_{\mathrm{L0}}^* R_0^{*3}}.\end{aligned} \tag{28}$$

The incident frequency $\omega^* \approx 11\,\mathrm{MHz}$ and phase velocity $U^* \approx 618\,\mathrm{m\,s^{-1}}$ for the case of a micrometer bubble (i.e., $R_0^* = 1\,\mu\mathrm{m}$) are examples of the order estimation of scale using Albunex (see Table 1). In this paper, we do not discuss the effect of dual frequency (Zhang and Li, 2017; Zhang, 2018), chaotic oscillations (Hegedüs and Klapcsik, 2015), and many complex aspects of bubble dynamics.

Furthermore, the nondimensional liquid viscosity, shell shear viscosity , viscosity describing the friction losses due to volume change, shell shear modulus, shell bulk modulus, and shell thickness are defined using ϵ (Chabouh et al., 2021; Kikuchi and Kanagawa, 2021):

$$\begin{aligned}&\frac{\mu_{\mathrm{L}}^*}{\rho_{\mathrm{L0}}^* U^{*2} T^*} = \epsilon\mu_{\mathrm{L}} \quad \frac{\mu_{\mathrm{S}}^*}{\rho_{\mathrm{L0}}^* U^{*2} T^*} = \mu_{\mathrm{S}}, \quad \frac{\mu_{\mathrm{K}}^*}{\rho_{\mathrm{L0}}^* U^{*2} T^*} = \mu_{\mathrm{K}},\\ &\frac{G^*}{\rho_{\mathrm{L0}}^* U^{*2}} = G, \quad \frac{K^*}{\rho_{\mathrm{L0}}^* U^{*2}} = K, \quad \frac{d_0^*}{R_0^*} = \epsilon d_0,\end{aligned} \tag{29}$$

where μ_{L}, μ_{S}, μ_{K}, G, K, and d_0 are constants of $O(1)$.

3. Derivation of KdVB equation

3.1. Leading order of approximation

Substituting Eqs. (19)–(29) into Eqs. (1) and (10)–(15) and equating the coefficients of like powers of ϵ in the resultant equations, the following set of linearized equations are obtained as first-order equations:

(i) The mass conservation equation for the gas phase,

$$\frac{\mathrm{D}\alpha_1}{\mathrm{D}t_0} - 3\frac{\mathrm{D}R_1}{\mathrm{D}t_0} + \frac{\partial u_1}{\partial x_0} = 0, \tag{30}$$

(ii) The mass conservation equation for the liquid phase,

$$\alpha_0\frac{\mathrm{D}\alpha_1}{\mathrm{D}t_0} - (1-\alpha_0)\frac{\partial u_1}{\partial x_0} = 0, \tag{31}$$

(iii) The momentum conservation equation for the gas phase,

$$(1-\alpha_0)\frac{\mathrm{D}u_1}{\mathrm{D}t_0} - \alpha_0 u_0\frac{\mathrm{D}\alpha_1}{\mathrm{D}t_0} + u_0(1-\alpha_0)\frac{\partial u_1}{\partial x_0} + \frac{\partial p_{\mathrm{L1}}}{\partial x_0} = 0, \tag{32}$$

(iv) The equation of motion for spherically symmetric oscillations of an encapsulated bubble,

$$\frac{\Delta^2}{\Omega^2}R_1 + p_{\mathrm{L1}} = C. \tag{33}$$

Here, the constant term C appears on the right-hand side of Eq. (33) in the present study, although this term did not appear in Kikuchi and Kanagawa (2021), is given by

$$C = \frac{3d_0}{3K+4G}\left\{4G[(3\gamma-1)p_{\mathrm{G0}} - 3K] + (3\gamma p_{\mathrm{G0}} - \sigma_1)^2 - 3K(3\gamma p_{\mathrm{G0}} - \sigma_1)\right\}, \tag{34}$$

where

$$\sigma_1 = \frac{2\sigma_1^*}{\rho_{\mathrm{L0}}^* U^{*2} R_0^*}. \tag{35}$$

Eliminating α_1, u_1, and p_{L1} from Eqs. (30)–(33), the single linear wave equation for first-order perturbation of bubble radius, R_1, is obtained:

$$\frac{\mathrm{D}^2 R_1}{\mathrm{D}t_0^2} - v_{\mathrm{p}}^2\frac{\partial^2 R_1}{\partial x_0^2} = 0, \tag{36}$$

with the phase velocity v_{p},

$$v_{\mathrm{p}} = \sqrt{\frac{\Delta^2/\Omega^2}{3\alpha_0(1-\alpha_0)}}. \tag{37}$$

Thus, the viscosity and elasticity of the shell do not contribute ultrasound propagation in the leading order of approximation. Setting $v_{\mathrm{p}} = 1$ gives the explicit form of U^* as

$$U^* = \sqrt{\frac{R_0^{*2}\omega_{\mathrm{B}}^{*2}}{3\alpha_0(1-\alpha_0)}}. \tag{38}$$

Focusing on the right-running wave alone, a phase function φ_0 is introduced as

$$\varphi_0 \equiv x_0 - (v_{\mathrm{p}} + u_0)t_0. \tag{39}$$

The other first-order perturbations are obtained from Eqs. (30)–(33) using φ_0:

$$\alpha_1 = s_1 R_1 = 3(1-\alpha_0)R_1, \tag{40}$$

$$u_1 = s_2 R_1 = -3\alpha_0 v_{\mathrm{p}} R_1, \tag{41}$$

Table 1
Physical properties of the shell (i.e., the shear modulus G_{S}^* [MPa], shell viscosity μ_{S}^* [Pa s], and shell thickness d_{S0}^* [nm]) for four major contrast agents: Albunex (Church, 1995), SonoVue (Tu et al., 2009), and Optison (Chatterjee and Sarkar, 2003). Levovist (Andersen and Jensen, 2009), and Optison (Chatterjee and Sarkar, 2003). According to surface tensions in Church (1995), $\sigma_1 = 0.04\,\mathrm{N/m}$ and $\sigma_2 = 0.05\,\mathrm{N/m}$ are used. These values are used in Figs. 3–7.

UCA	G_{S}^* [MPa]	μ_{S}^* [Pa s]	d_{S0}^* [nm]	References
Albunex	15	0.05	15	Church (1995)
SonoVue	20	0.6	4	Tu et al. (2009)
Levovist	80	1.3	6	Andersen and Jensen (2009)
Optison	20.7	1.7	7.5	Chatterjee and Sarkar (2003)

$$p_{L1} = s_3 R_1 + C = -3\alpha_0(1-\alpha_0)v_p^2 R_1 + C. \tag{42}$$

The main difference to our previous study can be observed in Eqs. (33) and (42). The explicit form of U^* (or v_p) coincides with the counterpart in our previous study for free bubbles; noting that U^* is implicitly affected the shell properties, since the eigenfrequency of bubble ω_B^* in U^* depends on the shell properties [see Eq. (28)]. Thus, the second order of approximation is considered. Therefore, if the shell is incompressible (i.e., $K \to \infty$) and there is an absence of initial flow velocity (i.e., $u_0 = 0$), $\mathrm{D}/\mathrm{D}t_0$ becomes $\partial/\partial t_0$, and the present result is almost identical to Kikuchi and Kanagawa (2021).

3.2. Second order of approximation and the resultant equation

Similar to the case of the leading order of approximation, the following single inhomogeneous equation for R_2 is derived as the second-order equation:

$$\begin{aligned}\frac{\mathrm{D}^2R_2}{\mathrm{D}t_0^2} - v_p^2\frac{\partial^2 R_2}{\partial x_0^2} = &-\frac{1}{3}\frac{\mathrm{D}K_1}{\mathrm{D}t_0} + \frac{1}{3\alpha_0}\frac{\mathrm{D}K_2}{\mathrm{D}t_0} + \frac{u_0}{3\alpha_0(1-\alpha_0)}\frac{\partial K_2}{\partial x_0} + \frac{1}{3\alpha_0(1-\alpha_0)}\frac{\partial K_3}{\partial x_0}\\ &- \frac{\Delta^2}{3\alpha_0(1-\alpha_0)\Omega^2}\frac{\partial^2 K_4}{\partial x_0^2} = K(R_1;\varphi_0,t_1,x_1),\end{aligned} \tag{43}$$

with the inhomogeneous terms K_i $(i = 1,2,3,4)$:

$$K_1 = -\frac{\partial u_1}{\partial x_1} + 3\frac{\mathrm{D}R_1}{\mathrm{D}t_1} - \frac{\mathrm{D}\alpha_1}{\mathrm{D}t_1} + 3\frac{\mathrm{D}R_1\alpha_1}{\mathrm{D}t_0} - 6\frac{\mathrm{D}R_1^2}{\mathrm{D}t_0} + 3\frac{\partial R_1 u_1}{\partial x_0} - \frac{\partial \alpha_1 u_1}{\partial x_0}, \tag{44}$$

$$K_2 = (1-\alpha_0)\frac{\partial u_1}{\partial x_1} - \alpha_0\frac{\mathrm{D}\alpha_1}{\mathrm{D}t_1} - \alpha_0\frac{\partial \alpha_1 u_1}{\partial x_0} + (1-\alpha_0)\frac{\mathrm{D}\rho_{L1}}{\mathrm{D}t_0}, \tag{45}$$

$$\begin{aligned}K_3 = &-u_0(1-\alpha_0)\tfrac{\partial u_1}{\partial x_1} - \tfrac{\partial p_{L1}}{\partial x_1} - (1-\alpha_0)\tfrac{\mathrm{D}u_1}{\mathrm{D}t_1} + \alpha_0 u_0\tfrac{\mathrm{D}\alpha_1}{\mathrm{D}t_1}\\ &-(1-\alpha_0)\tfrac{\partial u_1^2}{\partial x_0} + \alpha_0 u_0\tfrac{\partial \alpha_1 u_1}{\partial x_0} + \alpha_0\tfrac{\mathrm{D}\alpha_1 u_1}{\mathrm{D}t_0}\\ &-(1-\alpha_0)u_0\tfrac{\mathrm{D}\rho_{L1}}{\mathrm{D}t_0} + \tfrac{4}{3}(1+\alpha_0)\mu_L\tfrac{\partial^2 u_1}{\partial x_0^2},\end{aligned} \tag{46}$$

$$\begin{aligned}K_4 = &\left[1+\tfrac{3\gamma(3\gamma-1)\Omega^2 p_{G0}}{2\Delta^2}\right]R_1^2 - \Omega^2\tfrac{\mathrm{D}^2R_1}{\mathrm{D}t_0^2} - \Delta V\tfrac{\mathrm{D}R_1}{\mathrm{D}t_0} + 4\tfrac{\mu_L\Omega^2}{\Delta^2}\tfrac{\mathrm{D}R_1}{\mathrm{D}t_0}\\ &+4\tfrac{\Omega^2 d_0}{\Delta^2}\left[\mu_S\left(1-\tfrac{4G}{3K+4G}\right)+2\mu_K\tfrac{3G}{3K+4G}\right]\tfrac{\mathrm{D}R_1}{\mathrm{D}t_0}\\ &-\tfrac{\Omega^2 d_0 R_1}{\Delta^2}\left\{\tfrac{12Gp_{G0}}{3K+4G} + \left(1-\tfrac{12G}{3K+4G}\right)\sigma_1 - \tfrac{3}{3K+4G}\left[(3\gamma p_{G0}-\sigma_1)^2 - 3K(3\gamma p_{G0}-\sigma_1)\right]\right\}\\ &+\tfrac{\Omega^2}{\Delta^2}C_2.\end{aligned} \tag{47}$$

From the solvability condition of the inhomogeneous equation in Eq. (43), $K = 0$ is imposed (Kanagawa et al., 2010). By using Eq. (19), the independent variables φ_0, t_1, and x_1 in Eq. (43) are restored into t and x:

$$\begin{aligned}&\frac{\partial R_1}{\partial t} + (v_p + u_0)\frac{\partial R_1}{\partial x}\\ &+\epsilon\left(\Pi_0\frac{\partial R_1}{\partial x} + \Pi_1 R_1\frac{\partial R_1}{\partial x} + \Pi_2\frac{\partial^2 R_1}{\partial x^2} + \Pi_3\frac{\partial^3 R_1}{\partial x^3}\right)\\ &= 0,\end{aligned} \tag{48}$$

via the variables transform

$$\tau \equiv \epsilon t, \quad \xi \equiv x - (v_p + u_0 + \epsilon\Pi_0)t. \tag{49}$$

The KdVB equation is finally obtained in the following format:

$$\frac{\partial f}{\partial \tau} + \Pi_1 f\frac{\partial f}{\partial \xi} - \Pi_2\frac{\partial^2 f}{\partial \xi^2} + \Pi_3\frac{\partial^3 f}{\partial \xi^3} = 0. \tag{50}$$

Here, constant coefficients are given by

$$\begin{aligned}\Pi_0 = &-\tfrac{v_p(1-\alpha_0)\Delta^2 V^2}{6\alpha_0\Omega^2} - \tfrac{d_0}{6\alpha_0(1-\alpha_0)v_p}\left\{\tfrac{12G}{3K+4G}p_{G0} + \left(1-\tfrac{12G}{3K+4G}\right)\sigma_1\right.\\ &\left.-\tfrac{3}{3K+4G}\left[(3\gamma p_{G0}-\sigma_1)^2 - 3K(3\gamma p_{G0}-\sigma_1)\right]\right\}\end{aligned} \tag{51}$$

$$\Pi_1 = \frac{1}{6}\left[k_1 - \frac{k_2}{\alpha_0} + \frac{k_3}{\alpha_0(1-\alpha_0)} - 6v_p k_4\right], \tag{52}$$

$$\Pi_2 = \Pi_{21} + \Pi_{22} + \Pi_{23} + \Pi_{24} + \Pi_{25}, \tag{53}$$

$$\Pi_3 = \frac{v_p\Delta^2}{6\alpha_0(1-\alpha_0)} = \frac{\omega^{*2}}{2\epsilon\omega_B^{*2}}, \tag{54}$$

where Π_1 is composed of

$$k_1 = 6v_p(2-s_1) + 2s_2(3-s_1), \tag{55}$$

$$k_2 = -2\alpha_0 s_1 s_2, \tag{56}$$

$$k_3 = 0, \tag{57}$$

$$k_4 = 1 + \frac{\gamma(3\gamma-1)p_{G0}}{2\alpha_0(1-\alpha_0)v_p^2}, \tag{58}$$

and Π_2 is composed of

$$\Pi_{21} = \frac{2(1+\alpha_0)}{3(1-\alpha_0)}\mu_L, \tag{59}$$

$$\Pi_{22} = \frac{2}{3\alpha_0(1-\alpha_0)}\mu_L, \tag{60}$$

$$\Pi_{23} = \frac{2}{3\alpha_0(1-\alpha_0)}\mu_S\left(1-\frac{4G}{3K+4G}\right)d_0, \tag{61}$$

$$\Pi_{24} = \frac{4}{3\alpha_0(1-\alpha_0)}\mu_K\frac{3G}{3K+4G}d_0, \tag{62}$$

$$\Pi_{25} = \frac{1}{6\alpha_0(1-\alpha_0)}\frac{\Delta^3 V}{\Omega^2}. \tag{63}$$

Here, the absolute values of Π_0, Π_1, Π_2, and Π_3 represent the magnitude of advection, nonlinear, dissipation (i.e., attenuation), and dispersion effects, respectively. In Π_2, Π_{21} describes dissipation due to viscosity of the bulk liquid, Π_{22} describes dissipation due to liquid viscosity at the interface, Π_{23} describes dissipation due to shell viscosity, Π_{24} describes dissipation due to shell compressibility, and Π_{25} term describes dissipation due to liquid compressibility. Here, Π_2 and Π_3 are positive, while Π_0 and Π_1 are negative. It should be noted that the analytical expression of the signs of Π_0 and Π_1 is challenging. The present coefficient $\Pi_i\,(i = 0,1,2,3)$ does not depend on the initial void fraction α_0.

Although the present advection, nonlinear, and dissipation coefficients differ from our previous coefficients for free bubbles (Kanagawa et al., 2010), the dispersion coefficient Π_3 is identical to that in our previous coefficient (Kanagawa et al., 2010). As in the case of v_p or U^*, noting that the presence of shell does not affect explicitly the dispersion coefficient Π_3 (i.e., dispersion effect) of ultrasound; Π_3 implicitly depends on the presence of shell since ω_B^* in Π_3 depends on the shell [see Eqs. (28) and (54)]. If the shell is incompressible, Eq. (50) is almost identical to that in Kikuchi and Kanagawa (2021).

The shell compressibility, shell shear modulus, surface tension, and shell viscosity affect the advection, nonlinear, and dissipation terms (i.e., advection, nonlinear, and dissipation effects of ultrasound). A quantitative discussion is presented in the next section.

4. Discussion

Here, the advection, nonlinear, and dissipation coefficients of KdVB equation are quantitatively discussed based on the physical properties of four well-known UCAs: Albunex, SonoVue, Levovist, and Optison, summarized in Table 1. Noting that the shell thickness d_0^* is constant.

Figs. 3–5 show the advection, nonlinear, and dissipation coefficients Π_0, Π_1, and Π_2 versus the initial bubble radius R_0^*, respectively. The present coefficients for the case with shell compressibility are then compared to the previous coefficients for the cases without shells (Kanagawa et al., 2010) and without shell compressibility. Here, we defined without shell case as $\sigma_1^* = 0.072$ N/m, $\sigma_2^* = 0$, and $d_0^* = 0$. Figs. 3(a)–5(a) represent the case of Albunex as an example; the tendency was qualitatively identical for the case of the other UCAs.

4.1. Comparison amoung UCAs

From Fig. 3(b), the advection effect (i.e., absolute value of Π_0) of SonoVue is the smallest. Especially, $R_0^* = 1\,\mu$m for a medical use, the maximum value (i.e., Albunex) is approximately twice the minimum value (i.e., SonoVue). For the nonlinear coefficient Π_1, the difference between all UCAs increases with increasing R_0^*. The absolute value of SonoVue is the largest of all UCAs with shell compressibility [Fig. 4(b)]. Meanwhile, for the dissipation coefficient Π_2, the difference between all UCAs relatively increases with decreasing R_0^*; in particular, Optison has the largest difference of all UCAs with shell compressibility [Fig. 5(b)]. However, the order of sizes of four UCAs changes in the region of $R_0^* \leqslant 1\,\mu$m.

4.2. Five dissipation factors

Fig. 6 represents the components of Π_2 as follows: (i) Brown curve: Component of the viscosity of bulk liquid (i.e., Π_{21}); (ii) Orange curve: Component of the liquid viscosity at the interface (i.e., Π_{22}); (iii) Green curve: Component of the shell shear viscosity μ_S (i.e., Π_{23}); (iv) Red curve: Component of the shell viscosity describing the friction losses due to volume change μ_K (i.e., Π_{24}); and (v) Purple curve: Component of liquid compressibility (i.e., Π_{25}). It should be noted that the order of sizes of four UCAs changes in the region of $R_0^* \leqslant 1\,\mu$m.

In order of size, there are two types in $R_0^* = 1\,\mu$m: Type A (Albunex, Levovist, and Optison) has the highest shell compressibility, followed by the shell viscosity, liquid viscosity at the interface, liquid compressibility, and viscosity of bulk liquid, in that order; Type B (SonoVue) has the highest shell compressibility, followed in order by the liquid viscosity at interface, shell viscosity, liquid compressibility, and viscosity of bulk liquid. In both types, the dissipation due to the viscosity of bulk liquids is almost 2% that of the second lowest component of dissipation, even at $R_0^* = 10\,\mu$m.

4.3. Effect of shell

As can be observed in the absolute values in Figs. 3–5, the presence of the shell increases the advection and dissipation effects but decrease the nonlinear effect (i.e., absolute value of coefficients) as in our previous study for free bubbles (Kanagawa et al., 2010).

For the advection coefficient Π_0, the difference between the case considering shell compressibility and the case without the shell is almost constant regardless of changes in R_0^* [see blue and green curves in Fig. 3(a)]. For the nonlinear coefficient $|\Pi_1|$, the case of without shell is greater than the case of with shell case. Note that the present model ignored buckling and rupture, which

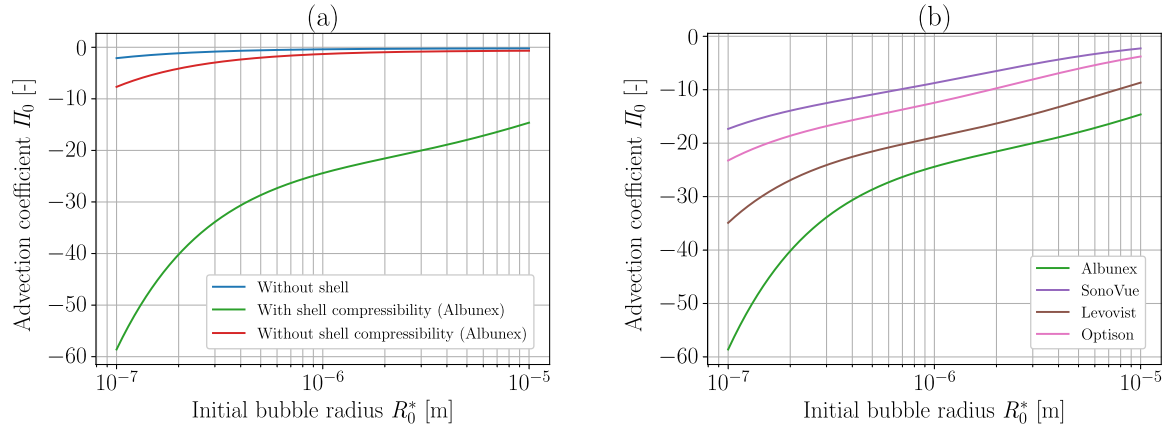

Fig. 3. Advection coefficient Π_0 versus the initial bubble radius R_0^* [m] for Optison, Albunex, SonoVue, and Levovist, without shell compressibility and without shell: $\Omega = 1, \sqrt{\epsilon} = 0.15, p_{L0}^* = 101325\,\mathrm{Pa}, \rho_{L0}^* = 1000\,kg/\mathrm{m}^3, c_{L0}^* = 1500\,\mathrm{m/s}, \mu_L^* = 1 \times 10^{-3}\,Pa \cdot \mathrm{s}, \mu_K^* = 0.7\mu_S^*, K^* = 0.7G^*, \alpha_0 = 0.005$. The other values are summarized in Table 1. These values are also used in Figs. 4–6. (a) Albunex with and without shell compressibility and without shell. (b) Optison, Albunex, SonoVue, and Levovist with shell compressibility.

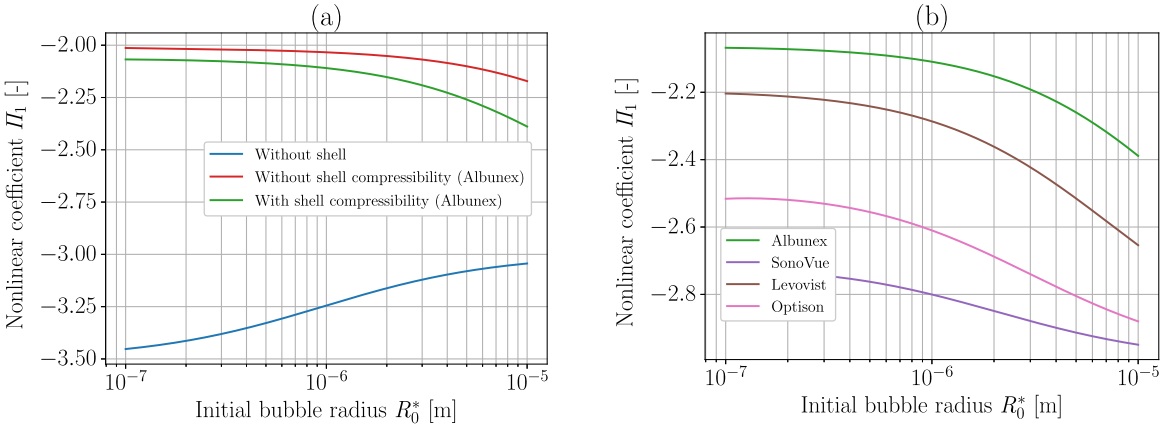

Fig. 4. Nonlinear coefficient Π_1 versus the bubble radius R_0^* [m]: (a) Albunex with and without shell compressibility and without shell; (b) Optison, Albunex, SonoVue, and Levovist with shell compressibility.

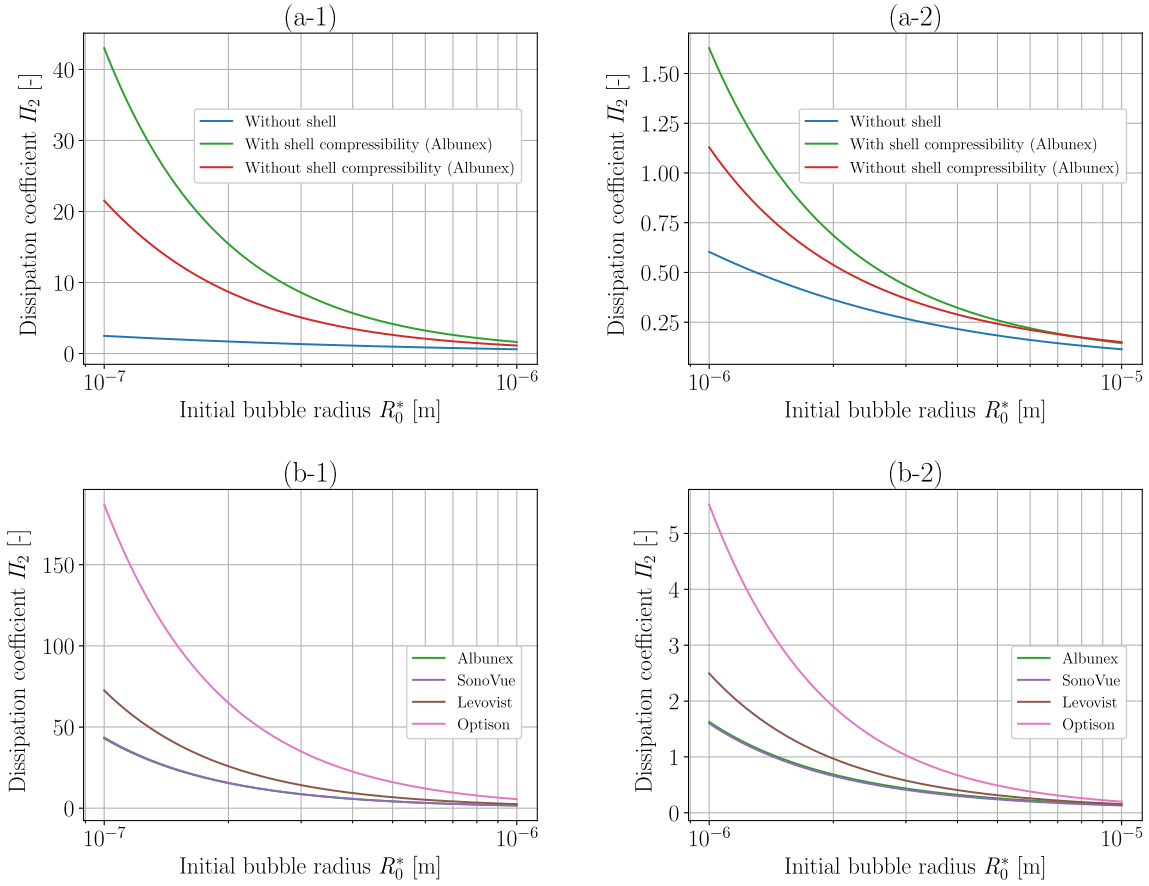

Fig. 5. Dissipation coefficient Π_2 versus the initial bubble radius R_0^* [m]: (a) Albunex with and without shell compressibility and without shell; (b) Optison, Albunex, SonoVue, and Levovist with shell compressibility. Note that the difference between SonoVue and Albunex is quite small.

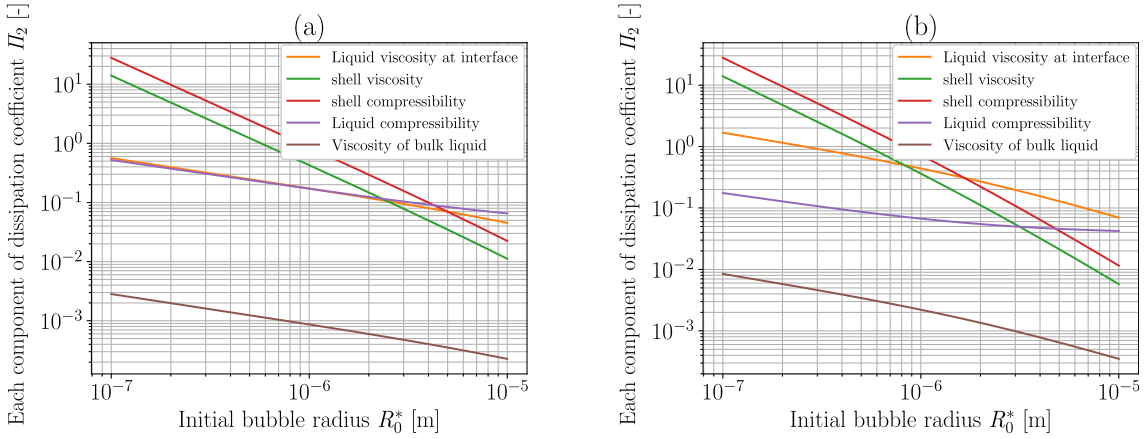

Fig. 6. Components of dissipation coefficient Π_2 of viscosity of bulk liquid (i.e., Π_{21}), liquid viscosity at the interface (i.e., Π_{22}), shell viscosity (i.e., Π_{23}), shell compressibility (i.e., Π_{24}), and liquid compressibility (i.e., Π_{25}): (a) Type A (Albunex) and (b) Type B (SonoVue).

increase the nonlinearity (Marmottant et al., 2005; Sojahrood et al., 2021c, 2021f) [see blue and green curves in Fig. 4(a)]. It is implied that the absolute value of the previously obtained nonlinear coefficient (Kikuchi and Kanagawa, 2021) neglecting shell compressibility will produce an overestimated value.

Meanwhile, for the dissipation coefficient Π_2, the difference between the two cases increases with decreasing R_0^* [see blue and green curves in Fig. 5(a)].

4.4. Effect of shell compressibility

In this study, an understanding of the effect of shell compressibility has been obtained for the first time. The following results show the importance of considering shell compressibility.

A greater advection coefficient Π_0 is observed in the case with shell compressibility than in the case without, and the difference between the two cases decreases with increasing R_0^*.

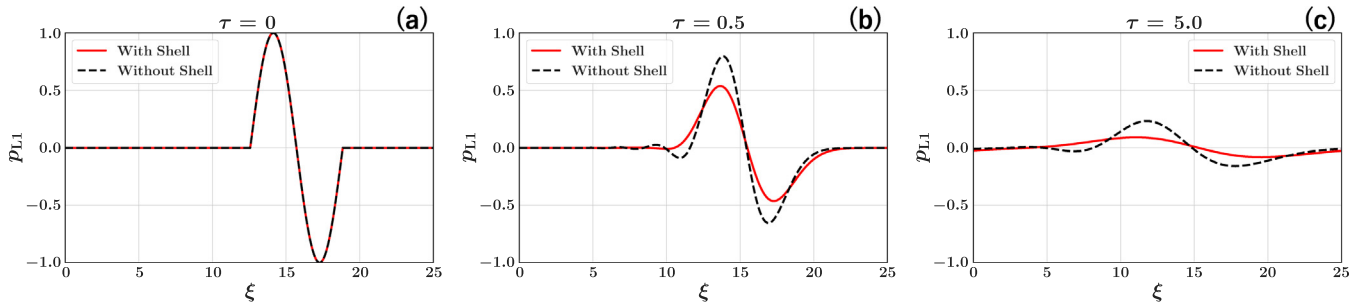

Fig. 7. Temporal evolution of the numerical solutions of the KdVB equation. The black and red curves represent the waveforms with shell compressibility case and, without shell case, respectively. The initial void fraction is $\alpha_0 = 0.01$ and the initial bubble radius is $R_0^* = 0.001\,\mathrm{mm}$. The nondimensional times are (a) $\tau = 0$, (b) $\tau = 0.5$, and (c) $\tau = 5.0$.

In $0.1\,\mu\mathrm{m} \leqslant R_0^* \leqslant 7\,\mu\mathrm{m}$, the dissipation coefficient Π_2 is greater in the case with shell compressibility than in the case without, and the difference decreases with increasing R_0^* [see red and green curves in Fig. 5(a)]. Note that the shell thickness, d_0^* is constant, the nondimensional number d_0 $(= d_0^*/R_0^*)$ decreases as increase R_0^*. This decreasing tendency of the overall shell effect with a decreasing d_0 agrees with the case of a single encapsulated bubble (Chabouh et al., 2021). The nonlinear coefficient Π_1 is lower in the case without shell compressibility than the case with [see red and green curves in Fig. 4(a)]. In summary, the consideration of shell compressibility (Chabouh et al., 2021) is important.

4.5. Limitation of present model

The present KdVB equation [Eq. (50)] was derived by the perturbation analysis up to second-order approximation. The present dissipation coefficient is composed as linear combination of each factor, and cannot describe nonlinear dissipation effect (Louisnard, 2012; Sojahrood et al., 2020b, 2020c, 2021b). For the case that the pressure amplitude becomes higher, nonlinear dissipation effect (Sojahrood et al., 2020b, 2020c, 2021b), is important. In a forthcoming paper, we will derive nonlinear dissipation coefficient (term) via a perturbation analysis with over third-order approximation.

Although the buckling and rupture will be occur (Marmottant et al., 2005; Sojahrood et al., 2021a, 2021c) when the pressure amplitude become higher, they are ignored in the present study. The effect of buckling and rupture will also be incorporated in a forthcoming paper. In light of the importance of bubble dynamics inside blood vessels, the interaction of encapsulated bubbles with vessels will also be analyzed (Hosseinkhah et al., 2013, 2014; Sassaroli and Hynynen, 2005; Vlachomitrou and Pelekasis, 2021a, 2021b).

4.6. Numerical example

Finally, we numerically solve the KdVB equation [Eq. (50)] to discuss the temporal- and spatial-evolutions of the waveform. The numerical scheme is a split-step Fourier method [the detail was shown in Appendix in our previous report (Kamei et al., 2021)]. The initial waveform is the sine pulse wave in Fig. 7(a). Here we depict the variation of liquid pressure, p_{L1} via the use of Eq. (42).

Fig. 7 shows the example of numerical solution. The solid red curve and dashed black curve represent the cases with and without the shell, respectively. The solid red curve was more attenuated than the dashed black curve because the dissipation effect is significant in the case of with shell [Eq. (50)]. The dashed black curve was distorted at $\xi \approx 10$ due to the dispersion effect, while the solid red curve was smooth due to the significant dissipation effect [Fig. 7(c)].

5. Conclusions

In this study, the weakly nonlinear propagation of one-dimensional ultrasound waves in a compressible liquid uniformly containing multiple encapsulated microbubbles was theoretically studied. The shell of the bubble is assumed to be a visco-elastic body (Kelvin–Voigt model). Furthermore, for the first time shell compressibility has been considered by utilizing a recently proposed equation of motion (Chabouh et al., 2021). The purpose of the study was to extend the acoustic theory of a single encapsulated bubble (Chabouh et al., 2021) to multiple encapsulated bubbles. To this end, our previous theory (Kikuchi and Kanagawa, 2021) was successfully extended to incorporate the viscosity of bulk liquid, shell compressibility, and liquid compressibility neglected in Kikuchi and Kanagawa (2021). The shell compressibility affected the advection, nonlinear, and dissipation terms, but did not contribute the dispersion term in the KdVB equation.

Focusing on the coefficients of advection, nonlinear, and dissipation terms, the following results were obtained: (i) The shell compressibility significantly increases the advection and dissipation effect, but slightly increases the nonlinear effect. The shell compressibility describes the friction losses due to volume change [the fourth term in Eq. (53)] increased the effects of the dissipation of ultrasound waves; (ii) From the comparison among four typical UCAs (i.e., Albunex, SonoVue, Levovist, and Optison), the different tendencies of the dissipation coefficient components were clarified; (iii) For the case of SonoVue, and Levovist, the dissipation coefficient due to shell compressibility was greater than that due to other factors at $R_0^* = 1\,\mu\mathrm{m}$ for medical use. In contrast, the dissipation coefficient due to the viscosity of bulk liquid was smaller than that due to other factors.

From these results, a basic understanding of the effect of the shell of encapsulated bubbles on nonlinear propagation of ultrasound waves was successfully obtained. We discover that the effect of shell compressibility, which has long been neglected, is absolutely necessary and requires discussion. A detailed comparison of the present model and the experimental results will be presented in a forthcoming paper.

Declaration of Competing Interest

The authors declare that they have no known competing financial interests or personal relationships that could have appeared to influence the work reported in this paper.

Acknowledgement

This work was partially carried out with the aid of the JSPS KAKENHI (18K03942), the Casio Science Promotion Foundation, and the Hattori Hokokai Foundation. We would like to thank four referees for their valuable comments and suggestions, Mitsuhiro Honda for his cooperation, and Editage (www.editage.com) for English language editing.

References

Akhatov, I., Parlitz, U., Lauterborn, W., 1994. Pattern formation in acoustic cavitation. J. Acoust. Soc. Am. 96, 3627.
Andersen, K.S., Jensen, J.A., 2009. Ambient pressure sensitivity of microbubbles investigated through a parameter study. J. Acoust. Soc. Am. 126, 3350.
Arai, S., Kanagawa, T., Ayukai, T., 2022. Nonlinear pressure waves in bubbly flows with drag force: Theoretical and numerical comparison of acoustic and thermal and drag force dissipations. J. Phys. Soc. Jpn. 91, 043401. https://doi.org/10.7566/JPSJ.91.043401.
Bader, K.B., Haworth, K.J., Shekhar, H., Maxwell, A.D., Peng, T., McPherson, D.D., Holland, C.K., 2016. Efficacy of histotripsy combined with rt-PA in vitro. Phys. Med. Biol. 61, 5253.
Boek, E.S., Padding, J.T., den Otter, W.K., Briels, W.J., 2005. Mechanical properties of surfactant bilayer membranes from atomistic and coarse-grained molecular dynamics simulations. J. Phys. Chem. 109, 19851.
Borden, M.A., 2019. Intermolecular forces model for lipid microbubble shells. Langmuir 35, 10042.
Chabouh, G., Dollet, B., Quilliet, C., Coupier, G., 2021. Spherical oscillations of encapsulated microbubbles: Effect of shell compressibility and anisotropy. J. Acoust. Soc. Am. 18, 1240.
Chatterjee, D., Sarkar, K., 2003. A Newtonian rheological model for the interface of microbubble contrast agents. Ultrasound Med. Biol. 29, 1749.
Choi, S.J., Schowalter, W.R., 1975. Rheological properties of nondilute suspensions of deformable particles. Phys. Fluids 18, 420.
Choi, J.J., Selert, K., Vlachos, F., Wong, A., Konofagou, E.E., 2011. Noninvasive and localized neuronal delivery using short ultrasonic pulses and microbubbles. PNAS 108, 16539.
Chong, W.K., Papadopoulou, V., Dayton, P.A., 2018. Imaging with ultrasound contrast agents: current status and future. Abdom. Radiol. 43, 762.
Christiansen, C., Kryvi, H., Sontum, P.C., Skotland, T.L., 1994. Physical and biochemical characterization of Albunex, a new ultrasound contrast agent consisting of air-filled albumin microspheres suspended in a solution of human albumin. Biotechnol. Appl. Biochem 19, 307.
Church, C.C., 1995. The effects of an elastic solid surface layer on the radial pulsations of gas bubbles. J. Acoust. Soc. Am. 97, 1510.
Cohen, J.L., Cheirif, J., Segar, D.S., Gillam, L.D., Gottdiener, J.S., Hausnerova, E., Bruns, D.E., 1998. mproved left ventricular endocardial border delineation and opacification with OPTISON (FS069), a new echocardiographic contrast agent: Results of a phase III multicenter trial. J. Am. Coll. Cardiol. 32, 746.
Cosgrove, D., Harvey, C., 2009. Clinical uses of microbubbles in diagnosis and treatment. Med. Biol. Eng. Comput. 47, 813.
Coussios, C.C., Roy, R.A., 2008. Applications of acoustics and cavitation to noninvasive therapy and drug delivery. Annu. Rev. Fluid Mech. 40, 395.
de Jong, N., Hoff, L., Skotland, T., Bom, N., 1992. Absorption and scatter of encapsulated gas filled microspheres: Theoretical considerations and some measurements. Ultrasonics 30, 95.
de Leon, A., Perera, R., Hernandez, C., Cooley, M., Jung, O., Jeganathan, S., Abenojar, E., Fishbein, G., Sojahrood, A.J., Emerson, C., Stewart, P.L., Kolios, M.C., Exner, A. A., 2019. Contrast enhanced ultrasound imaging by nature-inspired ultrastable echogenic nanobubbles. Nanoscale 11, 15647.
Dijkhuizen, W., van Sint Annaland, M., Kuipers, J.A.M., 2010. Numerical and experimental investigation of the lift force on single bubbles. Chem. Eng. Sci. 65, 1274.
Doinikov, A.A., Dayton, P.A., 2007. Maxwell rheological model for lipid-shelled ultrasound microbubble contrast agents. J. Acoust. Soc. Am. 121, 3331.
Doinikov, A.A., Haac, J.F., Dayton, P.A., 2009. Modeling of nonlinear viscous stress in encapsulating shells of lipid-coated contrast agent microbubbles. Ultrasonics 49, 269.
Einstein, A., 1906. Eine neue Bestimmung der Moleküldimensionen. Ann. Phys. 324, 289.
Entzian, K., Aigner, A., 2021. Drug delivery by ultrasound-responsive nanocarriers for cancer treatment. Pharmaceutics 13, 1135.
Fateh, S.T., Moradi, L., Kohan, E., Hamblin, M.R., Dezfuli, A.S., 2021. Comprehensive review on ultrasound-responsive theranostic nanomaterials: mechanisms, structures and medical applications. Beilstein J. Nanotechnol. 12, 808.
Ferrara, K., Pollard, R., Borden, M., 2007. Ultrasound microbubble contrast agents: Fundamentals and application to gene and drug delivery. Annu. Rev. Biomed. Eng. 9, 415.
Frinking, P.J.A., de Jong, N., 1998. Acoustic modeling of shell-encapsulated gas bubbles. Ultrasound Med. Biol. 24, 523.
Fuster, D., Conoir, J.M., Conoir, T., 2014. Effect of direct bubble-bubble interactions on linear-wave propagation in bubbly liquids. Phys. Rev. E 90, 063010.
Gorce, J.M., Arditi, M., Schneider, M., 2000. Influence of bubble size distribution on the echogenicity of ultrasound contrast agents: A study of SonoVue. Invest. Radiol. 35, 661.
Gubaidullin, D.A., Gubaidullina, D.D., Fedorov, Y.U., 2021a. Acoustics of a viscoelastic medium with encapsulated bubbles. J. Hydrodynamics 33, 55.
Gubaidullin, D.A., Gubaidullina, D.D., Fedorov, Y.U., 2021b. Radial oscillations of a shell-covered gas bubble in a viscoelastic liquid. Lobachevskii J. Math. 42, 2124.
Guédra, M., Cornu, C., Inserra, C., 2017. A derivation of the stable cavitation threshold accounting for bubble-bubble interactions. Ultrason. Sonochem. 38, 168.
Haghi, H., Sojahrood, A.J., Kolios, M.C., 2019. Collective nonlinear behavior of interacting polydisperse microbubble clusters. Ultrason. Sonochem. 58, 104708.
Hegedüs, F., Klapcsik, K., 2015. The effect of high viscosity on the collapse-like chaotic and regular periodic oscillations of a harmonically excited gas bubble. Ultrason. Sonochem. 27, 153.
Hissanaga, A.M., Padoin, N., Paladino, E.E., 2020. Mass transfer modeling and simulation of a transient homogeneous bubbly flow in a bubble column. Chem. Eng. Sci. 218, 115531.
Hoff, L., Sontum, P.C., Hovem, J.M., 2000. Oscillations of polymeric microbubbles: Effect of the encapsulating shell. J. Acoust. Soc. Am. 107, 2272.
Hosseinkhah, N., Chen, H., Matula, T.J., Burns, P.N., Hynynen, K., 2013. Mechanisms of microbubble-vessel interactions and induced stresses: a numerical study. J. Acoust. Soc. Am. 134, 1875.
Hosseinkhah, N., Goertz, D.E., Hynynen, K., 2014. Microbubbles and blood brain barrier opening: A numerical study on acoustic emissions and wall stress predictions. IEEE Trans. Biomed. Eng. 62, 1293.
Ignee, A., Atkinson, N.S.S., Schuessler, G., Dietrich, C.F., 2016. Ultrasound contrast agents. Endosc. Ultrasound 5, 355.
Ishii, M., 1977. One-dimensional drift-flux model and constitutive equations for relative motion between phases in various two-phase flow regimes. ANL Report, No. ANL-77-47.
Jeffrey, A., Kawahara, T., 1982. Asymptotic Methods in Nonlinear Wave Theory. Pitman, London.
Kamei, T., Kanagawa, T., Ayukai, T., 2021. An exhaustive theoretical analysis of thermal effect inside bubbles for weakly nonlinear pressure waves in bubbly liquids. Phys. Fluids 33, 053302.
Kanagawa, T., 2015. Two types of nonlinear wave equations for diffractive beams in bubbly liquids with nonuniform bubble number density. J. Acoust. Soc. Am. 137, 2642.
Kanagawa, T., Ayukai, T., Kawame, T., Ishitsuka, R., 2021b. Weakly nonlinear theory on pressure waves in bubbly liquids with a weak polydispersity. Int. J. Multiphase Flow 142, 103622.
Kanagawa, T., Ayukai, T., Maeda, T., Yatabe, T., 2021a. Effect of drag force and translation of bubbles on nonlinear pressure waves with a short wavelength in bubbly flows. Phys. Fluids 33, 053314.
Kanagawa, T., Kamei, T., 2021. Thermal effect inside bubbles for weakly nonlinear pressure waves in bubbly liquids: Theory on short waves. Phys. Fluids 33, 063319.
Kanagawa, T., Yano, T., Watanabe, M., Fujikawa, S., 2010. Unified theory based on parameter scaling for derivation of nonlinear wave equations in bubbly liquids. J. Fluid Sci. Technol. 5, 351.
Kanagawa, T., Yano, T., Watanabe, M., Fujikawa, S., 2011. Nonlinear wave equation for ultrasound beam in nonuniform bubbly liquids. J. Fluid Sci. Technol. 6, 279.
Kataoka, I., 1991. Modelling and basic equations of gas-liquid two-phase flow. Jpn. J. Multiphase Flow 5, 175.
Kerboua, K., Merouani, S., Hamdaoui, O., Alghyamah, A., Islam, M.H., Hansen, H.E., Pollet, B.G., 2021. How do dissolved gases affect the sonochemical process of hydrogen production? An overview of thermodynamic and mechanistic effects – On the "hot spot theory". Ultrason. Sonochem. 72, 105422.
Kikuchi, Y., Kanagawa, T., 2021. Weakly nonlinear theory on ultrasound propagation in liquids containing many microbubbles encapsulated by visco-elastic shell. Jpn. J. Appl. Phys. 60, SDDD14.
Kok, H.P., Cressman, E.N.K., Ceelen, W., Brace, C.L., Ivkov, R., Grull, H., ter Haar, G., Wust, P., Crezee, J., 2020. Heating technology for malignant tumors: a review. Int. J. Hyperth. 37, 711.
Kooiman, K., Vos, H.J., Versluis, M., De Jong, N., 2014. Acoustic behavior of microbubbles and implications for drug delivery. Adv. Drug Deliv. Rev 72, 28.
Lajoinie, G., Linnartz, E., Kruizinga, P., de Jong, N., Stride, E., van Soest, G., Versluis, M., 2017. Laser-driven resonance of dye-doped oil-coated microbubbles: A theoretical and numerical study. J. Acoust. Soc. Am. 141, 4.
Lau, Y.M., Bai, W., Deen, N.G., Kuipers, J.A.M., 2014. Numerical study of bubble break-up in bubbly flows using a deterministic Euler–Lagrange framework. Chem. Eng. Sci. 108, 9.
Lentacker, I., De Smedt, S.C., Sanders, N.N., 2009. Drug loaded microbubble design for ultrasound triggered delivery. Soft Matter 5, 2161.
Liu, Y., Sugiyama, K., Takagi, S., 2016. On the interaction of two encapsulated bubbles in an ultrasound field. J. Fluid Mech. 804, 58.
Louisnard, O., 2012. A simple model of ultrasound propagation in a cavitating liquid. Part I: Theory, nonlinear attenuation and traveling wave generation. Ultrason. Sonochem. 19, 56.
Maeda, T., Kanagawa, T., 2020. Derivation of weakly nonlinear wave equations for pressure waves in bubbly flows with different types of nonuniform distribution of initial flow velocities of gas and liquid phases. J. Phys. Soc. Jpn. 89, 114403.
Ma, J., Yu, J., Fan, Z., Zhu, Z., Gong, X., Du, G., 2004. Acoustic nonlinearity of liquid containing encapsulated microbubbles. J. Acoust. Soc. Am. 116, 186.

Ma, J., Chahine, G.L., Hsiao, T.S., 2015. Spherical bubble dynamics in a bubbly medium using an Euler–Lagrange model. Chem. Eng. Sci. 128, 64.
Marmottant, P., van der Meer, S., Emmer, M., Versluis, M., de Jong, N., Hilgenfeldt, S., Lohse, D., 2005. A model for large amplitude oscillations of coated bubbles accounting for buckling and rupture. J. Acoust. Soc. Am. 118, 3499.
Morgan, K.E., Allen, J.S., Dayton, P.A., Chomas, J.E., Klibaov, A.L., Ferrara, K.W., 2000. Experimental and theoretical evaluation of microbubble behavior: effect of transmitted phase and bubble size. IEEE T. Ultrason. Ferr. 47, 1494.
Murai, Y., Shiratori, T., Kumagai, I., Ruhs, P.A., Fischer, P., 2015. Effective viscosity measurement of interfacial bubble and particle layers at high volume fraction. Flow Meas. Instrum. 41, 121.
Park, S., Yoon, H., Emelianov, S., Aglyamov, S., 2017. Fluid flow measurement for diagnosis of ventricular shunt malfunction using nonlinear responses of microbubbles in the contrast-enhanced ultrasound imaging. Jpn. J. Appl. Phys. 56, 07JF10.
Paul, S., Katiyar, A., Sarkar, K., Chatterjee, D., Shi, W.T., Forsberg, F., 2010. Material characterization of the encapsulation of an ultrasound contrast microbubble and its subharmonic response: Strain-softening interfacial elasticity model. J. Acoust. Soc. Am. 127, 3846.
Postema, M., Gilja, O.H., 2011. Contrast-enhanced and targeted ultrasound. World J. Gastroenterol. 17, 28.
Prosperetti, A., 1991. The thermal behaviour of oscillating gas bubbles. J. Fluid Mech. 222, 587.
Qin, S., Caskey, C.F., Ferrara, K.W., 2009. Ultrasound contrast microbubbles in imaging and therapy: physical principles and engineering. Phys. Med. Biol. 54, R27.
Raymond, J.L., Haworth, K.J., Bader, K.B., Radhakrishnan, K., Griffin, J.K., Huang, S.L., McPherson, D.D., Holland, C.K., 2014. Broadband attenuation measurements of phospholipid-shelled ultrasound contrast agents. Ultrasound Med. Biol. 40, 410.
Renaud, G., Bosch, J.G., van der Steen, A.F.W., de Jong, N., 2012. Chirp resonance spectroscopy of single lipid-coated microbubbles using an ‘‘acoustical camera”. J. Acoust. Soc. Am. 132, EL470.
Roovers, S., Segers, T., Lajoinie, G., Deprez, J., Versluis, M., De Smedt, S.C., Lentacker, I., 2019. The role of ultrasound-driven microbubble dynamics in drug delivery: From microbubble fundamentals to clinical translation. Langmuir 35, 10173.
Sankaranarayanan, K., Sundaresan, S., 2002. Lift force in bubbly suspensions. Chem. Eng. Sci. 57, 3521.
Sarkar, K., Shi, W.T., Chatterjee, D., Forsberg, F., 2005. Characterization of ultrasound contrast microbubbles using in vitro experiments and viscous and viscoelastic interface models for encapsulation. J. Acoust. Soc. Am. 118, 12.
Sassaroli, E., Hynynen, K., 2005. Resonance frequency of microbubbles in small blood vessels: a numerical study. Phys. Med. Biol. 50, 5293.
Schowalter, W.R., Chaffey, C.E., Brenner, H., 1968. Rheological behavior of a dilute emulsion. J. Colloid Interface Sci. 26, 152.
Segers, T., De Jong, N., Versluis, M., 2016. Uniform scattering and attenuation of acoustically sorted ultrasound contrast agents: Modeling and experiments. J. Acoust. Soc. Am. 140, 2506.
Segers, T., Kruizinga, P., Kok, M.P., Lajoinie, G., De Jong, N., Versluis, M., 2018. Monodisperse versus polydisperse ultrasound contrast agents: Non-linear response, sensitivity, and deep tissue imaging potential. Ultrasound Med. Biol. 44, 1482.
Sojahrood, A.J., Kolios, M.C., 2012. Classification of the nonlinear dynamics and bifurcation structure of ultrasound contrast agents excited at higher multiples of their resonance frequency. Phys. Lett. A 376, 2222.
Sojahrood, A.J., de Leon, A., Lee, R., Cooley, M., Abenojar, E., Kolios, M.C., Exner, A., 2021e. Toward precisely controllable acoustic response of shell-stabilized nanobubbles: High yield and narrow dispersity. ACS Nano 15, 4901.
Sojahrood, A.J., Earl, R., Kolios, M.C., Karshafian, R., 2020a. Investigation of the 1/2 order subharmonic emissions of the period-2 oscillations of an ultrasonically excited bubble. Phys. Lett. A 384, 126446.
Sojahrood, A.J., Falou, O., Earl, R., Karshafian, R., Kolios, M.C., 2015. Influence of the pressure-dependent resonance frequency on the bifurcation structure and backscattered pressure of ultrasound contrast agents: a numerical investigation. Nonlinear Dyn. 80, 889.
Kagami, S., Kanagawa, T., 2022. Weakly nonlinear propagation of focused ultrasound in bubbly liquids with a thermal effect: Derivation of two cases of Khokolov–Zabolotskaya–Kuznetsoz equations. Ultrason. Sonochem., 88, 105911. https://doi.org/10.1016/j.ultsonch.2022.105911.
Sojahrood, A.J., Li, Q., Haghi, H., Karshafian, R., Porter, T.M., and Kolios, M.C., 2018. Pressure dependence of the ultrasound attenuation and speed in bubbly media: theory and experiment. arXiv:1811.07788.
Sojahrood, A.J., Haghi, H., Rostam Shirazi, N., Kolios, M.C., Karshafian, R., 2021d. On the threshold of 1/2 order subharmonic emissions in the oscillations of ultrasonically excited bubbles. Ultrasonics 112, 106363.
Sojahrood, A.J., Haghi, H., Wegierak, D., Karshafian, R., Kolios, M.C., 2019. A simple method to analyze the super-harmonic and ultra-harmonic behavior of the acoustically excited bubble oscillator. Ultrason. Sonochem. 54, 99.
Sojahrood, A.J., Haghi, H., Karshafian, R., Kolios, M.C., 2021b. Classification of the major nonlinear regimes of oscillations, oscillation properties, and mechanisms of wave energy dissipation in the nonlinear oscillations of coated and uncoated bubbles. Phys. Fluids 33, 016105.
Sojahrood, A.J., Haghi, H., Kolios, M.C., Karshafian, R., 2021c. Nonlinear dynamics and bifurcation structure of ultrasonically excited lipid coated microbubbles. Ultrason. Sonochem. 72, 105405.
Sojahrood, A.J., Haghi, H., Li, Q., Porter, T.M., Karshafian, R., Kolios, M.C., 2020b. Nonlinear power loss in the oscillations of coated and uncoated bubbles: Role of thermal, radiation and encapsulating shell damping at various excitation pressures. Ultrason. Sonochem. 66, 105070.
Sojahrood, A.J., Haghi, H., Porter, T.M., Karshafian, R., Kolios, M.C., 2021f. Experimental and numerical evidence of intensified non-linearity at the microscale: The lipid coated acoustic bubble. Phys. Fluids 33, 072006.
Sojahrood, A.J., Haghi, H., Karshafian, R., Kolios, M.C., 2020c. Critical corrections to models of nonlinear power dissipation of ultrasonically excited bubbles. Ultrason. Sonochem. 66, 105089.
Sojahrood, A.J., Haghi, H., Karshafian, R., Kolios, M.C., 2021a. Nonlinear dynamics of acoustic bubbles excited by their pressure-dependent subharmonic resonance frequency: influence of the pressure amplitude, frequency, encapsulation and multiple bubble interactions on oversaturation and enhancement of the subharmonic signal. Nonlinear Dyn. 103, 429.
Stride, E., 2008. The influence of surface adsorption on microbubble dynamics. Phil. Trans. R. Soc A. 366, 2103.
ter Haar, G., 1999. Therapeutic ultrasound. Eur. J. Ultrasound 9, 3.
Tran, T.N., Shibata, D., Norisuye, T., Nakanishi, H., Tran-Cong-Miyata, Q., 2016. Determination of particle size distribution and elastic properties of silica microcapsules by ultrasound spectroscopy. Jpn. J. Appl. Phys. 55, 07KC01.
Tryggvason, G., Lu, J., 2015. Direct numerical simulations of flows with phase change. Chem. Eng. Sci. 15, 2.
Tsiglifis, K., Pelekasis, N.A., 2008. Nonlinear radial oscillations of encapsulated microbubbles subject to ultrasound: The effect of membrane constitutive law. J. Acoust. Soc. Am. 123, 4059.
Tu, J., Guan, J., Qiu, Y., Matula, T.J., 2009. Estimating the shell parameters of SonoVue® microbubbles using light scattering. J. Acoust. Soc. Am. 126, 2954.
Uddin, S.M.Z., Komatsu, D.E., Motyka, T., Petterson, S., 2021. Low-intensity continuous ultrasound therapies—A systemic review of current state-of-the-art and future perspectives. J. Clin. Med 10, 2698.
van Opheusden, J.H.J., Molenaar, J., 2011. Lipid aggregate formation at an oscillating bubble surface: A simulation study. Phys. Rev. E 83, 051606.
Vlachomitrou, M., Pelekasis, N., 2021a. Numerical study of the interaction between a pulsating coated microbubble and a rigid wall. I. Translational motion. Phys. Rev. Fluids 6, 013601.
Vlachomitrou, M., Pelekasis, N., 2021b. Numerical study of the interaction between a pulsating coated microbubble and a rigid wall. II. Trapped pulsation. Phys. Rev. Fluids 6, 013602.
Yano, T., Kanagawa, T., Watanabe, M., Fujikawa, S., 2013. Nonlinear Wave Propagation in Bubbly Liquids, Shock Wave. Science and Technology Reference Library, Springer, https://doi.org/10.1007/978-3-642-34297-4_4. pp. 107–140.
Yatabe, T., Kanagawa, T., Ayukai, T., 2021. Theoretical elucidation of effect of drag force and translation of bubble on weakly nonlinear pressure waves in bubbly flows. Phys. Fluids 33, 033315.
Yoshida, K., Tamura, K., Yamaguchi, T., 2016. Estimation of size and number density of microbubbles based on analysis of frequency-dependent attenuation. Jpn. J. Appl. Phys. 55, 07KC03.
Yoshizawa, S., Ikeda, T., Ito, A., Ota, R., Takagi, S., Matsumoto, Y., 2009. High intensity focused ultrasound lithotripsy with cavitating microbubbles. Med. Biol. Eng. Comput. 47, 851.
Zhang, Y., 2018. Chaotic oscillations of gas bubbles under dual-frequency acoustic excitation. Ultrason. Sonochem. 40, 151.
Zhang, Y., Li, S., 2014. Thermal effects on nonlinear radial oscillations of gas bubbles in liquids under acoustic excitation. Int. J. Heat Mass Transf. 53, 43.
Zhang, Y., Li, S., 2017. Combination and simultaneous resonances of gas bubbles oscillating in liquids under dual-frequency acoustic excitation. Ultrason. Sonochem. 35, 431.
Zhu, J., Tagawa, N., 2019. High resolution ultrasonic imaging based on frequency sweep in both of transducer element domain and imaging line domain. Jpn. J. Appl. Phys. 58, SGGE03.